Science
AAAS

Supplementary Materials for

Nucleosynthetic isotope anomalies of zinc in meteorites constrain the origin of Earth's volatiles

Rayssa Martins*†, Sven Kuthning†, Barry J. Coles, Katharina Kreissig, Mark Rehkämper*

Correspondence to: r.martins-pimentel19@imperial.ac.uk or markrehk@imperial.ac.uk

This PDF file includes:

Materials and methods
Supplementary Text
Figs. S1 to S10
Tables S1 to S11

Materials and methods

Samples

18 distinct meteorites were analyzed, with all relevant information, including meteorite sources, summarized in Table S1. The analyses encompassed (i) 11 carbonaceous chondrites (CC), of which one was a CI1 (Orgueil), two CM2s (including Murchison), three CV3s (including Allende) and one CO3; (ii) two EH enstatite chondrites (EC); (iii) seven ordinary chondrites (OC) of groups H, L and LL; and (iv) the IAB complex iron meteorites Canyon Diablo and Toluca.

Four rocks of the bulk silicate Earth (BSE) and 'Allende Matrix' samples were analyzed for quality control (Table S1). The BSE rocks encompass the United States Geological Survey (USGS) geological reference material BHVO-2, a Hawaiian basalt, as well as rock samples encompassing an Icelandic basalt from the Reykjanes Peninsula [BTHO, (*45*)], a gabbro from the Dufek Intrusion in Antarctica [D-174, (*46*)] and a glacial sediment from the west coast of Greenland [P6Bt, (*47*)]. These meteorites and the BSE rocks were either used up completely by destructive analysis during the course of the study (Orgueil, Jbilet Winselwan, Murchison, Allende, NWA 4502, MIL 090025, Brownfield (1937), Bishunpur, Soko Banja, Toluca, D-174) or remaining sample aliquots (LAR 12002, NWA 13299, Indarch, Forest Vale, Saratov, Tennasilm, Homestead, Canyon Diablo, BHVO-2, BTHO, P6Bt) are stored at the Department of Earth Science & Engineering, Imperial College London.

The Allende Matrix samples were obtained as follows. Aliquots of the Allende CV3 meteorite had their native Zn removed using the first stage ion exchange chemistry described below. The remaining solutions containing the meteorite matrix were then doped with the London Zn standard solution, dried down, and treated in a manner identical to that of other samples.

Laboratory and reagents

Digestion and further preparation of the samples and the subsequent Zn isotopic measurements were carried out in the Mass Spectrometry and Isotope Geochemistry (MAGIC) Laboratories at the Department of Earth Science & Engineering of Imperial College London. All sample preparation was conducted in ISO Class 6 clean rooms, using ISO Class 4 laminar flow benches for critical steps. The water used was of ≥18.2 MΩ cm quality from a Millipore purification system. All acids were purified from reagent grade stock acids by sub-boiling distillation in either quartz glass (15.3 M HNO_3, 6 M HCl) or Teflon (28 M HF, 12 M HCl, 8.5 M HBr) stills.

Initial sample treatment and digestion

Powder aliquots of the chondritic meteorites with masses of about 0.15 g to 10 g (Table S1) were obtained by crushing sample chips with an agate mortar and pestle. When present, fusion crusts were removed before crushing with a rotary tool and SiC grinding bits. For most meteorites, more than about 0.5 g of powder were digested to ensure sample homogeneity; for a few samples smaller powder aliquots from larger masses of homogenized powder were digested (Table S1).

The chondritic meteorites and BSE rocks were digested in Savillex Teflon beakers in a 2 + 1 mixture of 28 M HF + 15.3 M HNO_3 at 120° C for at least two days on a hotplate. Following this, the samples were dried, refluxed in 6 M HCl for at least another two days and dried again. Some samples (Orgueil CI1, Murchison CM2, Allende CV3) received additional treatment prior to refluxing in 6 M HCl. Allende CV3 was refluxed on a hotplate for several days with a 1 + 1 mixture of 15.3 M HNO_3 + 12 M HCl, followed by 15.3 M HNO_3, prior to being taken up in 6 M HCl . For Murchison and Orgueil, the additional digestion step was performed in Savillex beakers, which were heated in Parr Instrument Company bomb vessels with a 3 + 1 mixture of 15.3 M HNO_3 + 12 M HCl for four days at 135º C.

The Canyon Diablo sample was taken from a previous study (*48*). Prior to digestion, the metal slab was first abraded with SiC paper and then further cleaned by several acid leaching steps with intermittent H_2O rinses: (i) treatment with 0.5 M HBr in an ultrasonic bath for 1 hour; (ii) treatment with 6 M HCl in an ultrasonic bath for 1 hour; (iii) treatment with dilute aqua regia (3 parts 6 M HCl + 1 part 15.3 M HNO_3) in an ultrasonic bath for 15 min. Following leaching, the remaining metal was rinsed with H_2O and distilled ethanol. Finally, the remaining sample was transferred to a 60 ml Teflon beaker and completely digested by refluxing in 100 ml dilute aqua regia on a hot plate at 80º C for two days. The Toluca sample was obtained as a solution in aqua regia from an earlier study, which had applied aggressive cleaning of the metal by acid leaching prior to digestion (*48*). The aqua regia solutions of both iron meteorites were dried, and the residues refluxed in 6 M HCl for two days at 120° C and then dried again.

Anion exchange separation of Zn

The dried sample residues after digestion were re-dissolved in an appropriate volume of 3 M HCl by refluxing for ≥12 hr. Prior to the anion exchange chemistry, the sample solutions were cooled and centrifuged to remove any solid

residues. The three-stage anion exchange chromatography procedure was modified from published methods (*48-51*), as described in Tables S4 and S5. The first stage employed 100-200 mesh Bio-Rad AG-1X8 anion exchange resin, either in quartz glass columns with 2 ml resin beds or Teflon shrink-fit columns with 250 µl resin beds (Table S4). In both cases, the same acids were used for resin cleaning and equilibration as well sample loading and elution but with volumes scaled to the resin bed size (*50, 51*).

The Zn fractions from the first separation stage were dried and re-dissolved in 1 ml 1 M HCl for loading onto the columns of the second separation stage (Table S5). This second stage utilized Teflon shrink-fit columns with 250 µl of 100-200 mesh Bio-Rad AG-MP1 anion exchange resin, with a resin cleaning and elution procedure largely following published methods (*48, 49*) and described in detail in Table S5. The Zn fractions from the second-stage separation were dried, dried again with a few drops of 15.3 M HNO_3 and taken up in 1 ml 1 M HCl for the final stage of the Zn separation. This third stage was a duplicate of the second-stage column chemistry with 250 µl of 100-200 mesh Bio-Rad AG-MP1 anion exchange resin (Table S5). The Zn fractions from the stage 3 columns were dried, dried again after refluxing with 15.3 M HNO_3 and stored for the Zn isotope measurements.

Zn isotope measurements

All isotope analyses were carried out with a Nu Instruments Nu Plasma II multiple collector inductively coupled plasma mass spectrometer (MC-ICP-MS). A Nu Instruments DSN 100 desolvation system fitted with glass cross flow nebulizers with solution flow rates of about 120 µl min^{-1} were employed for sample introduction in conjunction with a CETAC ASX-112FR autosampler. Normal operating conditions are summarized in Table S6.

The Zn isotope analyses were carried out using two different Faraday cup configurations, termed M64 and M70, because the mass dispersion of the Nu Plasma II instrument did not permit simultaneous monitoring of all five Zn isotopes and the required interference monitors (Table S7). The M64 configuration covers the isotopes ^{64}Zn, ^{66}Zn, ^{67}Zn and ^{68}Zn as well as the ^{62}Ni monitor to correct for interferences from ^{64}Ni. The M70 configuration covers ^{66}Zn, ^{67}Zn, ^{68}Zn, ^{70}Zn and also monitors ^{72}Ge to correct for interferences from ^{70}Ge (Table S7). All ion beams were monitored using Faraday cups fitted with 10^{11} Ω resistors, with each run encompassing 3 blocks with 10 data acquisition cycles of 8 s each. Each run was started by a peak centering routine whilst each block commenced with a 60 s measurement of the electronic baselines of the Faraday collectors whilst the ion beam was deflected in the electrostatic analyzer.

For the measurements, samples and Zn reference materials were introduced as solutions in 0.1 M HNO_3 and this acid was also used for intermittent washing of the sample introduction system. The Zn isotope analyses with the M64 and M70 collector configurations were carried out at different Zn concentrations, as the fractional abundance of ^{70}Zn is much lower than that of ^{64}Zn, at about 0.6% versus 49.2% (Table S7). Measurements using the M64 and M70 configurations therefore utilized Zn concentrations of about 150 to 300 ng ml^{-1} and 250 to 400 ng ml^{-1}, respectively, depending on the instrumental sensitivity, which was normally 230 to 420 V $(\mu g\ ml^{-1})^{-1}$ for Zn.

All Zn isotope analyses were carried out with the sample–standard bracketing technique, whereby sample runs were symmetrically bracketed by two or four runs of a 'matching' solution of the London Zn isotope reference material. As the concentrations of the sample stock solutions were known, it was possible to prepare the sample run solutions with concentrations, which matched those of the bracketing London Zn isotope standards to within 10% to 15%.

Data reduction and presentation

The raw measured isotope ratios were corrected (during the measurements) for instrumental mass bias by internal normalization using the exponential law (*52*). Several different normalization schemes were originally trialed. Of these, normalization to $^{66}Zn/^{67}Zn$, with $^{66}Zn/^{67}Zn = 6.883939$ (*53*) best resolves the Zn isotope anomalies and was therefore adopted in most of our analyses. Data for this normalization scheme were collected with both the M64 and the M70 cup configurations and the combined results are shown in Figs. 1, 2, S2 and listed in Table S2. Additional results, obtained via internal normalization to $^{64}Zn/^{67}Zn = 12.170590$ (*53*) using only the M64 collector configuration, demonstrate the consistency of the data (Figs. S1, S4, Table S2).

Further results obtained with the M64 configuration are presented for internal normalization to $^{64}Zn/^{68}Zn = 2.665308$ [(*53*), Table S2]. This normalization avoids ^{67}Zn, which is particularly susceptible to nuclear field shift effects, and allows a comparison with the previously published Zn isotope data (*24*). The data collected in this manner are less suitable for resolving the expected and observed Zn isotope anomalies, so are not discussed in the main text. They are, however, discussed in a section below to evaluate whether the observed anomalies are a consequence of nuclear field shift effects.

The corrections for isobaric overlap of ^{64}Ni with ^{64}Zn and ^{70}Ge with ^{70}Zn were also carried out as part of the data reduction. They incorporate a correction for instrumental mass bias and employed ratios of ^{64}Ni/^{62}Ni = 0.254671 and ^{70}Ge/^{72}Ge = 0.74933 (*53*). As the ^{64}Zn/^{67}Zn normalization features ^{64}Zn, which is corrected for the presence of isobaric ^{64}Ni, an iterative procedure that optimizes both the mass bias and spectral interference corrections was employed for data reduction.

The Zn isotope data are reported using the ε notation, to denote deviations of the measured isotope ratio for a sample (sam) from the value determined for the London Zn reference standard (std) in parts per 10^4:

$$\varepsilon^{\mathrm{i/j}}Zn_{\mathrm{k/j}} = \left(\frac{(\,^{\mathrm{i}}Zn/\,^{\mathrm{j}}Zn)_{\mathrm{sam}}}{(\,^{\mathrm{i}}Zn/\,^{\mathrm{j}}Zn)_{\mathrm{std}}} - 1\right) x\ 10^4 \qquad \text{(S1)}$$

where i/j is the isotope ratio of interest and k/j the normalization ratio. As data obtained via the ^{66}Zn/^{67}Zn normalization scheme is most frequently quoted in the manuscript, a simplified ε^{i}Zn notation is adopted in this case. The full $\varepsilon^{\mathrm{i/j}}Zn_{\mathrm{k/j}}$ notation, however, is used to denote Zn isotope data normalized to ^{64}Zn/^{67}Zn and ^{64}Zn/^{68}Zn. In practice, the εZn values of samples were ubiquitously calculated relative to the mean isotopic results that were obtained for about 20 to 40 runs of the London Zn standard during the same measurement session.

Quality control of Zn isotope data

Zinc background levels (blanks) were highly variable (between about 30 and 300 ng) during the course of the study, mainly depending on the volume of digestion acids used (as dictated by sample size) and the methods employed for digestion and Zn separation. In all cases, however, the total Zn blanks were less than 1% of the Zn present in the samples, so no corrections were applied.

We investigated whether the Zn isotope anomalies determined for the meteorites are a consequence of analytical artefacts. Isobaric interferences from Ni during runs of samples (Ni/Zn ≈ 7.1×10^{-7} to 5.5×10^{-5}) and London Zn standards (Ni/Zn ≈ 7.4×10^{-7} to 2.5×10^{-5}) were consistently at similar levels and amounted to maximum interference corrections of ^{64}Ni/^{64}Zn ≈ 2×10^{-6}. For Ge, the interference levels were slightly higher but also almost identical for analyses of samples (Ge/Zn ≈ 9.4×10^{-6} to 5.8×10^{-5}) and London Zn solutions (Ge/Zn ≈ 9.6×10^{-6} to 5.8×10^{-5}), with a typical (median) Ge/Zn ≈ 2.2×10^{-5} for both. The median and maximum Ge interference levels are equivalent to interference corrections, as quantified by ^{70}Ge/^{70}Zn, of about 7×10^{-4} and 1.9×10^{-3}, respectively. As the εZn values of samples are determined relative to London Zn results obtained in the same measurement session and runs of doped solutions with larger interference levels of Ni/Zn = 1 x 10^{-4} and Ge/Zn = 3×10^{-4} did not produce any resolvable analytical biases, we regard the applied Ni and Ge interference corrections as robust.

Comprehensive mass scans that were routinely carried out on the Zn fractions of meteorite samples and in-run monitoring at mass numbers 62 (^{62}Ni, ^{46}Ti^{16}O) and 72 (^{72}Ge, ^{56}Fe^{16}O) demonstrate that other spectral interferences on Zn isotopes, from Ba^{2+} and molecular ions (e.g., $MgAr^+$, $AlAr^+$, $SiAr^+$, TiO^+, CrO^+, FeO^+) were at unproblematic levels. Interferences from Ba^{2+} ions could, in principle, be measured during the runs (e.g., by monitoring $^{137}Ba^{2+}$ at mass number 68.5) and corrected as part of the data reduction. We did not do so due to the following observations. Ba^{2+} monitors at mass numbers 67.5 and 68.5 yielded Ba^{2+} levels equivalent to $^{137}Ba^{2+}/^{137}Ba \approx 0.3$ for London Zn solutions, in accord with the Ba^{2+}/Ba^+ ratios of about 0.05 to 0.2 typically expected for Ba ionization in the plasma of quadrupole ICP-MS instruments (*54*). In contrast, the meteorite samples gave unexpectedly high ratios of $^{137}Ba^{2+}/^{137}Ba \approx 1.5$. As analyses of both sample and London Zn solutions ubiquitously showed similar Ba/Zn ratios of 1-2 × 10^{-5}, we expect actual Ba^{2+} interference levels on ^{66}Zn, ^{67}Zn and ^{68}Zn to be negligible at ≤1.5×10^{-6}. Given that samples and London Zn solutions had almost identical Ba/Zn ratios, no corrections for Ba^{2+} interferences were applied.

We performed multiple analyses of four different BSE rocks (Table S1) that together define a mean εZn value for the BSE that is identical to the expected result of εZn = 0 within 2se error, regardless of the internal normalization scheme that was used (Fig. S5, Table S2). Due to their compositions (with relatively high Ba, Al, Si, Ti and low Zn abundances), the BSE samples should suffer from larger spectral interferences from Ba^{2+} and many relevant molecular ions (Table S7) than the meteorites. Analyses of the synthetic 'Allende Matrix' samples also consistently yielded values of εZn = 0 (Fig. S5, Table S2).

The datasets obtained via internal normalization to ^{66}Zn/^{67}Zn and ^{64}Zn/^{67}Zn are fully consistent with one another. All CCs display Zn isotope anomalies that are complementary to those of the non-carbonaceous chondrites (ECs, OCs) and IAB complex irons, which is unlikely to be due to analytical artefacts (Figs. 1, 2, S1, S4; Table S2).

Modeling of nucleosynthetic isotope effects

To assess whether the observed Zn isotope anomalies are of nucleosynthetic origin they must link to a feasible stellar source which produces the minor neutron-rich ^{70}Zn isotope (0.6%), and ^{68}Zn and ^{66}Zn, without overproducing abundant ^{64}Zn (49.2%). All five stable Zn nuclides are produced by the weak s-process in the He-burning shells of massive stars and by alpha-rich freezeout at quasi-equilibrium conditions in supernovae explosions, with only minor contributions from the main s-process in low mass AGB stars (*55*). The ^{70}Zn yields of both the main and the weak s-process are too low to produce the ^{70}Zn enrichments observed for CCs (*56, 57*). Type II supernovae (SNII) have high production rates of ^{64}Zn, such that the observed ε^{64}Zn anomalies could be explained by an excess of SNII-derived pre-solar matter in the non-carbonaceous meteorites (*58*). This is, however, the opposite of what is seen for other Fe-peak element isotope anomalies, which are thought to result from a depletion of anomalous pre-solar matter in non-carbonaceous meteorites. The ^{68}Zn yields of SNII are highly sensitive to the mass of the star, such that both an excess or a deficit of this isotope can be produced relative to an excess of ^{70}Zn.

In contrast, both Type Ia supernovae (SNIa) and electron-capture supernovae (ECSNe) produce appreciable amounts of ^{66}Zn, ^{68}Zn and ^{70}Zn, with low yields of ^{64}Zn (*28, 30*). We then carried out modeling to assess whether the observed mass independent Zn isotope anomalies might reflect contributions of Zn produced in SNIa (*28*) or ECSNe (*30*). In the models, hypothetical materials with the isotopic composition of each nucleosynthetic source were mixed with baseline material that was assigned the BSE Zn isotope composition, which defined εZn = 0 in analyses of the London Zn isotope reference material (*53*).

For the ECSN model, the isotope abundances were taken from [(*30*), their figure 5] whilst the abundances employed in the SNIa model are from [(*28*), their table 4A]. The dilution factor employed was 1×10^{-6}, chosen to produce anomalies within the range of observed values (εZn < 5). The calculated isotope compositions were converted to εZn notation using Eq. 1. For both the ECSN and the SNIa model, the previous publications (*28, 30*) provide multiple isotope abundance estimates, which correspond to different assigned values for the ignition density. Thus, four trendlines were produced for the ECSN model, corresponding to the unchanged model, as well as the models in which the densities were multiplied by factors of ×1.3, ×2 and ×10 (Figure S6). Likewise, four trendlines were calculated for the SNIa model, namely NCD4A, NCD6A, NCD7A, and NCD8A (Figure S6). When isotope abundances were not given, they were assumed to be zero. The shaded areas in Figures 2, S4 and S9 correspond to the areas delimited by the trendlines with the lowest and highest gradients, which thus encompass the remaining two trendlines.

The same nucleosynthetic models that were employed for Zn were also used to generate hypothetical nucleosynthetic Ti and Cr isotope anomalies (Fig. S2). Subsequently, the slope of the expected correlations in plots of ε^{70}Zn vs. ε^{50}Ti and ε^{70}Zn vs ε^{54}Cr were determined from (*59*):

$$\varepsilon^{i/y}Zn_{x/y} = \frac{\rho_{Zn}^{i/y} - \rho_{Zn}^{x/y}\,\mu_{Zn}^{i/y}/\mu_{Zn}^{x/y}}{\rho_{E}^{j/b} - \rho_{E}^{a/b}\,\mu_{E}^{j/b}/\mu_{E}^{a/b}}\; c_{b_E}^{\;y_{Zn}}\; \varepsilon^{j/b}E_{a/b}, \qquad \text{(S2)}$$

with

$$\rho_{E}^{p/q} = (\,^{p}E/\,^{q}E)_{star}/(\,^{p}E/\,^{q}E)_{Sun} - 1 \qquad \text{(S3)}$$

where (^{p}E/ ^{q}E) denotes isotope ratios of the elements (E) Ti or Cr and Zn (when E = Zn) for either the modeled stellar source (star) or the Solar System (Sun);

$$\mu_{E}^{p/q} = \ln(m_{\,^{p}E}/m_{\,^{q}E}) \qquad \text{(S4)}$$

where ($m_{\,^{p}E}/m_{\,^{q}E}$) denote ratios of the exact atomic masses of Ti or Cr and Zn (when E = Zn);

$$c_{b_E}^{\;y_{Zn}} = (\,^{y}Zn/\,^{b}E)_{star}/(\,^{y}Zn/\,^{b}E)_{Sun} \qquad \text{(S5)}$$

where (^{y}Zn/ ^{b}E) is the ratio of a Zn to a Ti or Cr isotope for either the modeled stellar source (star) or the Solar System (Sun).

The average Ti and Cr isotope anomalies observed for each meteorite group were calculated based on the available literature, as summarized in Table S8 (*29, 34, 60*).

Mass balance calculations

Mean values and uncertainties

For individual meteorites and meteorite groups with only a single sample (CI, CO chondrites), the mean and 2sd (two standard deviations) were determined from the results of n individual runs; the respective 2se uncertainties were calculated as 2sd/√n, using the n individual sample runs. For other meteorite groups, the mean and 2sd values were determined from the mean values of x distinct meteorites in the group; the 2se errors were calculated as 2sd/√x for x distinct meteorites.

Modeling

The contributions of the carbonaceous and non-carbonaceous reservoirs to the bulk Earth (BE) Zn inventory were estimated based on a two-component mixture:

$$\varepsilon^{i}Zn_{BE} = x_{CC}^{Zn} \cdot \varepsilon^{i}Zn_{CC} + x_{NC}^{Zn} \cdot \varepsilon^{i}Zn_{NC} \quad \text{(S6)}$$

where x_{CC}^{Zn} and x_{NC}^{Zn} are the fractions of Zn derived from the CC and the non-carbonaceous (NC) material, respectively. To test whether the outcome of the modeling is affected by the selection of meteorites or by the isotope ratio used in the calculations, a total of eighteen models were generated, which each employed different meteorite endmembers and one of three isotope ratios (^{64}Zn, ε^{70}Zn and $\varepsilon^{66/67}Zn_{64/67}$). Three CC and four NC endmembers that encompass between one and five meteorite groups were tested, and their compositions were defined as the mean of their respective groups (Table S9).

The mixing between these endmembers was modeled using Monte Carlo simulations. With the exception of the combination described in the main text (CI-CM-CO-CV + EC-OC, ε^{64}Zn), which encompasses 10,000 trials, all other combinations were simulated with 1,000 trials. The endmember compositions were assigned by randomly generating numbers within ±2se of their means. Similarly, a random number between 0 and 1 was attributed to x_{CC}^{Zn}, and $x_{NC}^{Zn} = (1 - x_{CC}^{Zn})$. Earth's composition is defined by the London Zn reference material ($\varepsilon^{i}Zn_{BE} = 0$) and the uncertainty that is associated with the long-term reproducibility of the procedure, as characterized by analyses the four BSE samples (±0.17, ±0.74, and ±0.10 for ε^{64}Zn, ε^{70}Zn and $\varepsilon^{66/67}Zn_{64/67}$, respectively; Table S2). Only simulations which produced an $\varepsilon^{i}Zn_{BE}$ within these intervals (uncertainties) were considered successful.

The average x_{CC}^{Zn} values obtained from all simulations are identical within uncertainty (Table S10), with an overall mean of $x_{CC}^{Zn} \approx 0.52$. Although providing lower precision, the models that employed ε^{70}Zn or $\varepsilon^{66/67}Zn_{64/67}$ corroborate the results of models that employ our preferred isotope ratio, ε^{64}Zn. The results also demonstrate that the selection of meteorite groups has negligible impact on the outcome of the modeling. Even in an extreme scenario that employs only CM and H chondrites, which represent the least and most Earth-like groups within the CC and NC reservoirs, respectively, the fraction of CC-derived Zn that is needed to reproduce Earth's Zn isotope composition is 0.31 ± 0.15, 0.33 ± 0.37, and 0.31 ± 0.24 for ε^{64}Zn, ε^{70}Zn and $\varepsilon^{66/67}Zn_{64/67}$, respectively. This still overlaps, within the uncertainties, with our preferred estimate of 0.48±0.15. Similarly, if the most and least Earth-like CC and NC groups are used (CO and EH chondrites), the modeling yields x_{CC}^{Zn} values of 0.61 ± 0.17, 0.72 ± 0.34, and 0.61 ± 0.24 using ε^{64}Zn, ε^{70}Zn and $\varepsilon^{66/67}Zn_{64/67}$, respectively. Again, these results are compatible with our preferred x_{CC}^{Zn} estimate. Altogether, the models indicate that, to reproduce the Earth's Zn isotope composition, considerable Zn contributions from both the carbonaceous and the non-carbonaceous reservoir are required.

A similar approach was used to estimate the mass fraction of CC material accreted by the Earth (x_{CC}). In this case, two equations were employed:

$$\varepsilon^{i}Zn_{BE} = \frac{x_{CC} \cdot [Zn]_{CC} \cdot \varepsilon^{i}Zn_{CC} + x_{NC} \cdot [Zn]_{NC} \cdot \varepsilon^{i}Zn_{NC}}{x_{CC} \cdot [Zn]_{CC} + x_{NC} \cdot [Zn]_{NC}} \quad \text{(S7)}$$

and

$$[Zn]_{BE} = x_{CC} \cdot [Zn]_{CC} + x_{NC} \cdot [Zn]_{NC} \quad \text{(S8)}$$

The modeling then employed the same endmember meteorite group combinations and isotope ratios as were used in conjunction with Eq. S7 above (Table S11). The Zn concentration of the CC endmember was randomly chosen between 115 μg g^{-1} and 320μg g^{-1}, which correspond to the average compiled Zn abundances of the CO-CV and CI

groups, respectively (Table S3; the CM group has an intermediate Zn concentration). The same procedure was adopted for $[Zn]_{BE}$, which was allowed to range from 40 μg g^{-1} to 70 μg g^{-1}, due to uncertainty about how much Zn is sequestered in the core (Table S3). In contrast, the Zn concentration of the NC reservoir was treated as a free parameter. As above, only simulations which reproduced the BE Zn isotope composition (within error) were considered. The resulting x_{CC} averages are all identical within uncertainty (Table S11), with an overall mean of $x_{CC} \approx 0.14$ for all eighteen simulations. The successful simulations were also used to estimate the Zn concentration of the NC endmember, which yields a mean of 33 ± 15 μg g^{-1} for our preferred model (CI-CM-CO-CV + EC-OC, $\varepsilon^{64}Zn$), and identical results within uncertainty for all other models.

In summary, the results of all eighteen models are consistent, regardless of which Zn isotope ratio is employed or which meteorite groups are used as endmembers. This was further verified by an ANOVA test, which compared the x_{CC}^{Zn} and x_{CC} results obtained for the six different endmember combinations (Table S11). This test yielded p-values of 0.25 and 0.34 for x_{CC}^{Zn} and x_{CC}, respectively, which both exceed the critical value of $p_{crit} = 0.05$, indicating no evidence for statistically significant differences.

Further ANOVA tests were carried out to compare the Zn isotope compositions of individual meteorites within a given endmember (or 'meteorite grouping'; Table S9). These analyses also showed no significant isotopic differences within the different groupings, with p-values that exceed the critical value for all three isotope ratios, even when all available CCs and NCs are included (Table S9). In contrast, ANOVA tests comparing CCs with the non-carbonaceous meteorites (EC-OC-IAB) return p-values of 3×10^{-4}, 4×10^{-4}, and 2×10^{-21} for $\varepsilon^{64}Zn$, $\varepsilon^{70}Zn$ and $\varepsilon^{66/67}Zn_{64/67}$, respectively. The ANOVA analyses therefore show that the Zn isotope compositions of meteorites within the same CC or NC grouping are statistically indistinguishable, whilst typical CC and NC isotope compositions are statistically distinct from one another.

The limited variance in Zn isotope compositions within each reservoir contrasts with the diversity that is observed for other isotope systems. In particular, ECs and OCs have distinct nucleosynthetic Ti, Cr, Zr, Mo, and Ru isotope compositions [(*39*); Table S8], whilst the Mo and Ru isotope compositions of IAB complex irons are different from ECs and OCs (*39*). The same is true for CCs, which display large isotopic differences for some refractory element isotope systems [e.g., $\varepsilon^{94}Mo_{CI} = 0.79 \pm 0.41$ and $\varepsilon^{94}Mo_{CM} = 4.82 \pm 0.20$; (*39*)]. This could arise from a more homogeneous distribution of anomalous Zn within each reservoir than in the material that is responsible for the isotope anomalies of more refractory elements.

Supplementary Text

Mass dependent Zn isotope fractionation

Mass dependent Zn isotope variations in meteorites are commonly quantified using $\delta^{66}Zn$ values, which denote the difference of the $^{66}Zn/^{64}Zn$ isotope ratio of a sample from the JMC Lyon Zn isotope reference material in parts per 1000 (‰). Mass dependent Zn isotope data may provide additional constraints (i) on the carbonaceous versus non-carbonaceous origin of Earth's Zn and (ii) on whether the mass independent Zn isotope anomalies identified in this study (and possibly the volatile-depleted elemental abundances found in chondrites) reflect thermal processing.

Mass dependent Zn isotope data are not available for the meteorite powders that we analyzed. Coupled εZn-$\delta^{66}Zn$ results are available for seven meteorites (Orgueil CI1; Murchison, Jbilet Winselwan, CM2; Allende CV3; Brownfield (1937) H3.7; Bishunpur LL3.1; Indarch EH4) that were analyzed here for εZn and previously for $\delta^{66}Zn$ [Fig. S7; (*38, 61, 62*)].

The available mass dependent Zn isotope data for chondrites provide only limited constraints on the carbonaceous versus non-carbonaceous origin of Earth's Zn inventory. CCs, ECs and OCs display overlapping $\delta^{66}Zn$ values, whereby the data for the latter two meteorite groups are more variable (Fig. S7). This reflects that ECs and OCs are more impacted by secondary alteration within the parent asteroids, such that the bulk $\delta^{66}Zn$ values of the meteorite parent bodies are uncertain (*25, 38*). The $\delta^{66}Zn$ value estimated for the BSE overlaps with results published for CV and CO carbonaceous as well ordinary and enstatite chondrites [Fig. S7, (*36, 38, 61-66*)]. This provides no constraints on the source of Earth's Zn inventory as it could be derived to 100% from any of these meteorite groups or any mixture between them.

Correlation between εZn and $\delta^{66}Zn$ values for chondrites might be produced by thermal processing of primitive material in the early Solar System, with associated loss of phases that carry Zn (with a distinct nucleosynthetic isotope signature) and concomitant mass dependent Zn isotope fractionation. However, the available data offer no evidence for such a relationship (Fig. S7). For example, the $\delta^{66}Zn$ values of CI, CM, CO and CV chondrites are distinct but no

such differences are apparent for $\varepsilon^{64}Zn$ (Fig. S7). In addition, both ECs and OCs have highly variable $\delta^{66}Zn$ values, which record alteration of the original composition by subsequent parent body processes. The heavy Zn isotope compositions of many OCs and some ECs are most likely due to Zn mobilization and loss by thermal or shock metamorphism, with associated isotope fractionation (*25, 38*). Whilst the low $\delta^{66}Zn$ values of other OCs might record parent body compositions, as they cannot be the consequence of evaporative Zn loss, it is more likely that they reflect recondensation of mobilized Zn with associated isotope fractionation, as has been found for Cd isotopes (*50*). The $\delta^{66}Zn$ values of EC and OC meteorites are therefore unconstraining, as it is unclear if they are indicative of parent body compositions that are different from or identical to the compositions of the CC parent bodies.

Evaluation of nuclear field shift effects

In principle, it is possible that the Zn isotope anomalies are not of nucleosynthetic origin but a consequence of mass independent isotope fractionations from nuclear field shift effects (NFSEs). Such fractionations can be generated by the same processes and in the same settings that produce mass dependent isotope effects (*67*), but rather than being dictated by mass, NFSEs scale with the nuclear charge radii of the nuclei. Mass independent isotope fractionations are more evident for elements with high atomic masses (e.g., U, Tl, Hg) and are thought to become smaller with decreasing atomic mass (*68*). As such, they have not been detected in natural samples for elements with atomic numbers $Z < 80$ (Hg). However, it was previously proposed that NFSEs may be responsible for Mo, Ru, and Te isotope anomalies in bulk meteorites (*69, 70*). We therefore evaluated whether the Zn isotope signatures we measured in this study are possibly a consequence of NFSEs. In principle, the investigated samples could have acquired mass independent isotope fractionations from NFSEs in one of two settings. First, they could be an indigenous fingerprint of the meteorites that records Solar System processes. Second, the isotope fractionation could have occurred in the laboratory during processing of the meteorites. Both possibilities are discussed below.

Laboratory-induced NFSEs

Our data indicate systematic and complimentary mass independent Zn isotope effects for CCs versus non-carbonaceous meteorites, with an intermediate signature for Earth's Zn (Figs. 1, 2, S1, S4). We cannot envision how such systematic and consistent isotope effects could be generated by an analytical procedure, which is more likely to induce random analytical artefacts.

If mass independent isotope fractionation was to occur in the laboratory, the most likely origin would be the Zn separation by the column chemistry procedure (Tables S4, S5). This is because mass dependent isotope fractionation of Zn and other metals can occur during column chromatography if the yields are incomplete; mass independent isotope fractionation has been observed for Zn during such procedures (*71*). For most of our samples, the Zn yields during sample preparation (including column chemistry) were >80%. For a few samples, however, the yields were as low as 20%. No samples have a correlation between Zn yields and εZn values. For example, the aliquot of sediment sample P6Bt with the lowest Zn yield (of 42%) had $\varepsilon^{64}Zn = +0.13 \pm 0.46$ (2se, n = 4), consistent with the London Zn standard. Furthermore, the Allende aliquot with the lowest Zn yield (of 21%) produced a mean $\varepsilon^{64}Zn$ value (of -1.47 ± 0.42; 2se, n = 4) which is consistent with the overall Allende mean of $\varepsilon^{64}Zn = -0.91 \pm 0.21$ (2se, n = 51) that includes data for aliquots with yields exceeding 90%. This lack of correlation between Zn yields and the mass independent Zn isotope results leads us to conclude that the observed anomalies are unlikely to be an artefact of Zn loss and associated isotope fractionation during sample preparation.

Natural NFSEs

In principle, the systematic Zn isotope anomalies of CCs versus non-carbonaceous meteorites might originate from processes that induced mass independent Zn isotope fractionations from NFSEs in the protoplanetary disk.

If the complementary mass independent Zn isotope compositions of the outer and inner Solar System reservoirs were generated by NFSEs, such a dichotomy would also be expected for their mass dependent Zn isotope compositions. Whilst the $\delta^{66}Zn$ values of many enstatite and ordinary chondrites are not complementary to those of CCs, this does not provide conclusive evidence for the absence of large-scale isotope fractionation in the protoplanetary disk. Rather, it most likely reflects that the former meteorites were altered by secondary processes involving thermal mobilization of Zn on the parent bodies. In particular, both ECs and OCs display highly variable $\delta^{66}Zn$ values, which are thought to reflect different extents of evaporative Zn loss and associated mass dependent isotope fractionation during thermal and shock metamorphism (*25, 38*). However, if NFSEs were important for Zn, such parent body processes would have also impacted the mass independent Zn isotope compositions of the meteorites. However, our data show no resolvable differences in εZn values between ordinary chondrites that were subjected to different extents of thermal

metamorphism, as recorded by petrographic grades of between 3.1 and 5 (Fig. S8, Table S1). The data include results for two meteorites that differ substantially in their mass dependent Zn isotope composition with δ^{66}Zn values of –0.30 ± 0.05‰ (Brownfield (1937) H3.7) and 0.25 ± 0.05‰ (Bishunpur LL3.1) (Fig. S8). Furthermore, ANOVA tests conducted for the OCs show no statistically significant differences in the Zn isotope compositions of these meteorites (with $p > 0.15$, Table S9; see Methods and materials for further details about the ANOVA tests). We therefore consider it unlikely that the observed εZn anomalies are a consequence of mass independent Zn isotope fractionation which occurred during thermal processing of Solar System matter in the protoplanetary disk.

If the observed εZn anomalies are a consequence of NFSEs, they should follow predictions from models of NFSE-based mass independent isotope fractionation. The mass independent Zn isotope fractionation that results from NFSEs is given by (*67*):

$$\varepsilon^{i/y}\mathrm{Zn}_{x/y} = \left(\delta\langle r^2\rangle_{m_y,m_i} - \frac{m_x(m_i-m_y)}{m_i(m_x-m_y)}\delta\langle r^2\rangle_{m_y,m_x}\right)\cdot\alpha \quad \text{(S9)}$$

where the εZn value is obtained for isotope ratio (i/y), internally normalized to ratio (x/y) to correct for instrumental mass discrimination, m_i corresponds to the atomic mass of nuclei i, $\delta(r^2)_{my,mi}$ is the difference in mean-squared nuclear charge radii of the nuclei y and i, and α is a temperature-dependent and scalable parameter. We used nuclear charge radii data of (*72*) to determine εZn values obtained with internal normalization to ^{66}Zn/^{67}Zn and ^{64}Zn/^{68}Zn, and checked with alternative nuclear charge radii (*73*) for Zn isotope data measured with the ^{64}Zn/^{68}Zn normalization scheme (Fig. S9).

When Zn isotope data normalized to ^{66}Zn/^{67}Zn are evaluated, both the modeled NFSE trend and the trends predicted by the two nucleosynthetic models (see Materials and methods) match our measurements (Fig. S9). The similarity in the trends predicted by the NFSE and the nucleosynthetic models is because the nuclear configuration (which impacts nuclear volume and charge radius) is also linked to properties such as nuclear binding energy, which are relevant in nucleosynthetic processes (*68*). As NFSEs tend to generate the most prominent anomalies for nuclides with odd atomic mass numbers, results obtained using the ^{64}Zn/^{68}Zn normalization were also examined (Fig. S9). In this case, the $\varepsilon^{66/68}\mathrm{Zn}_{64/68}$ and $\varepsilon^{67/68}\mathrm{Zn}_{64/68}$ values of the meteorites show small but still resolvable anomalies, which are in accord with the modeled nucleosynthetic trends. However, most of the meteorite results are not compatible with the two NFSE trends, which predict larger $\varepsilon^{67/68}\mathrm{Zn}_{64/68}$ anomalies for a given value of $\varepsilon^{66/68}\mathrm{Zn}_{64/68}$, regardless of which set of nuclear charge radii data are used (Fig. S9). This confirms that the Zn isotope anomalies observed for meteorites are unlikely to be caused by NFSEs.

We compare our results to previously published mass independent Zn isotope data (*24*). Previous workers used ^{68}Zn/^{64}Zn for internal normalization, with isotope data reported using ^{64}Zn in the denominator, and found no evidence of mass independent Zn isotope effects in repeated analyses of five chondrites, encompassing three CCs, one EC and one OC. In contrast to (*24*), the current study employed ^{64}Zn/^{68}Zn for normalization and the isotope ratios are reported with ^{68}Zn in the denominator. Notably, the switching of the numerator and denominator isotopes in the normalization ratio has no impact on the results of the instrumental mass bias correction. Furthermore, identical εZn values are obtained for the two normalization schemes, regardless of whether the isotope ratios are reported using ^{64}Zn or ^{68}Zn in the denominator. As such, the $\varepsilon^{X/68}\mathrm{Zn}_{64/68}$ data of this study are directly comparable to the $\varepsilon^{X/64}\mathrm{Zn}_{68/64}$ results of *(24)*, shown in Fig. S9.

A comparison of the data acquired in this study and by (*24*) reveals that the results are largely compatible, with many overlapping Zn isotope patterns for CC and NC meteorites. The differences in conclusions between this study and ref (*24*) primarily reflects (i) differences in measurement precision; (ii) different numbers of samples investigated (iii) differing normalization scheme, whereby the magnitude of the expected nucleosynthetic isotope effect is relatively small compared to the analytical precision for some.

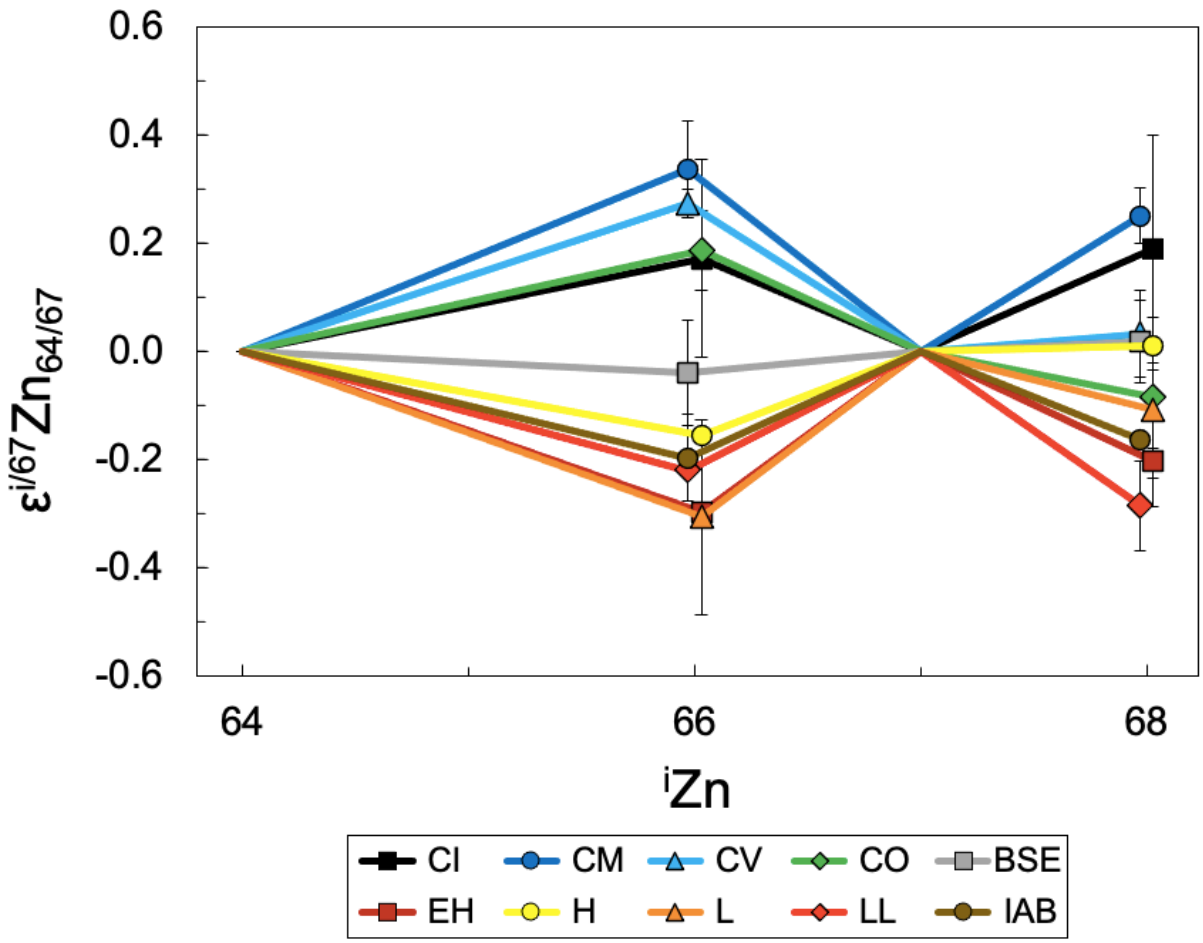


Figure S1. **Mass independent Zn isotope compositions measured using internal normalization to $^{64}Zn/^{67}Zn$.** Same as Figure 1, but for data obtained using $^{64}Zn/^{67}Zn$ for mass bias normalization.

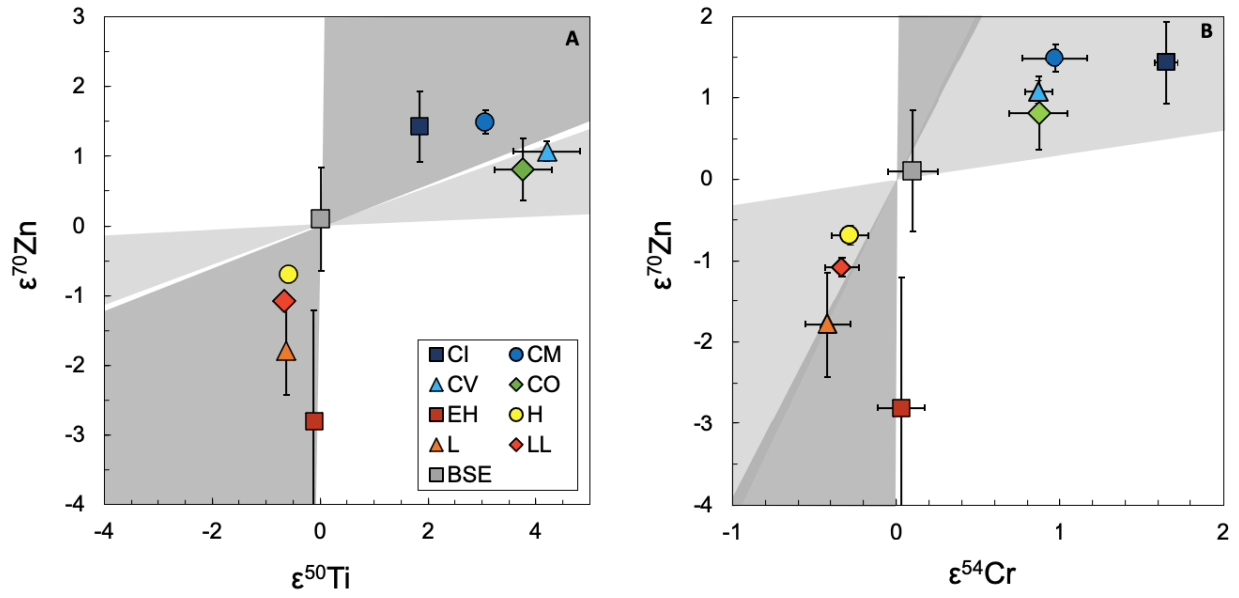


Figure S2. **Correlation between nucleosynthetic isotope anomalies of Zn and other Fe-peak elements.** (A) ε^{70}Zn versus ε^{50}Ti (Table S8) and (B) ε^{70}Zn versus ε^{54}Cr (Table S8) for CCs (CI, CM, CV, CO), ECs (EH) and OCs (H, L, LL); the BSE data give the mean result for the four BSE rocks. Predicted correlation between the anomalies for SNIa (light grey area) and ECSNe (dark grey area) are also shown (see Materials and methods). Previous work has shown a dichotomy in the ε^{50}Ti and ε^{54}Cr data of carbonaceous versus non-carbonaceous meteorites (*29, 34*). Whilst there is no clear correlation, the ε^{70}Zn data are in accord with this dichotomy. The combined results are also consistent with the modeled nucleosynthetic isotope anomalies, except for EHs which show no resolvable anomalies relative to the BSE for refractory elements, unlike for Zn. The ε^{70}Zn data for the meteorites and BSE rocks are from Table S2; the error bars show ±2se. The ε^{50}Ti and ε^{54}Cr data (and data sources) are in Table S8; error bars indicate ±2se.

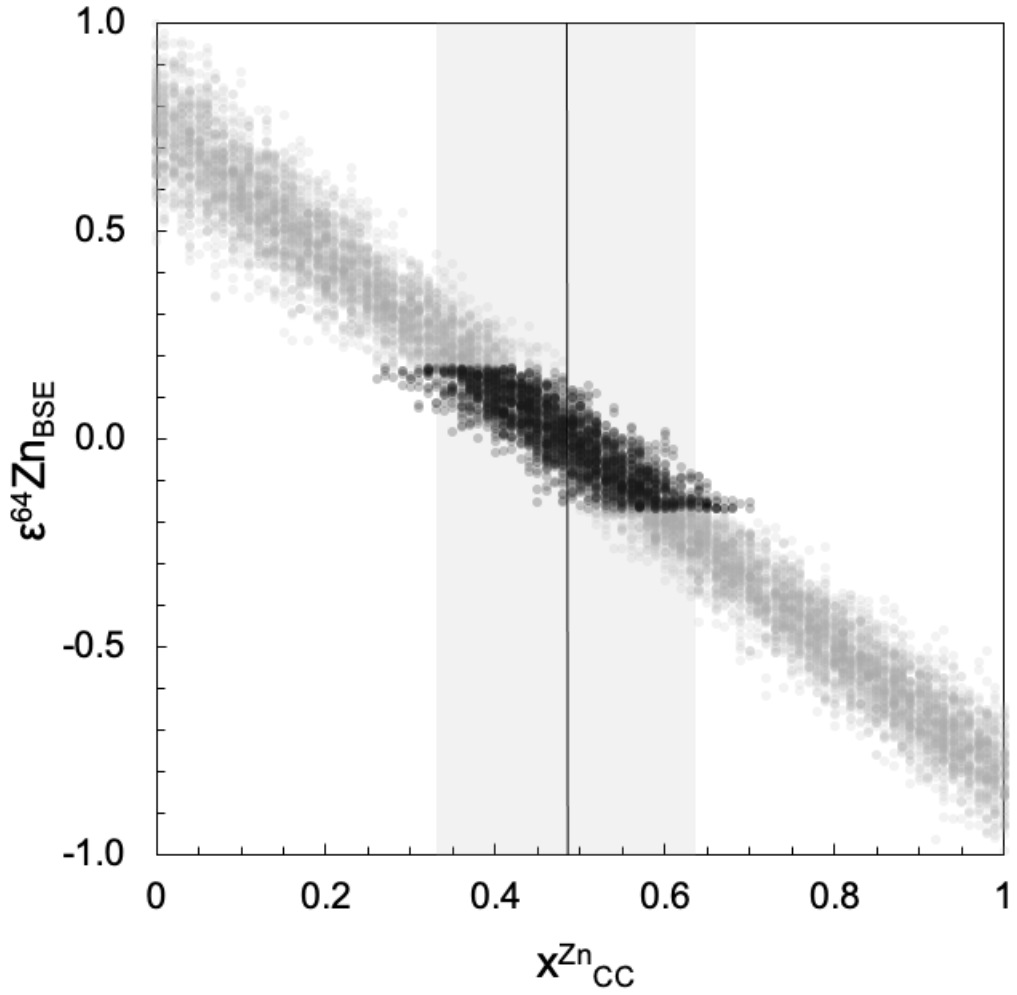


Figure S3. Inferred CC contribution to the bulk Earth Zn inventory from Monte Carlo simulations. The diagram plots the $\varepsilon^{64}Zn_{BE}$ values versus the Zn fractions derived from the CC reservoir (x^{Zn}_{CC}) as obtained from 10,000 mass balance simulations (see Materials and methods). Shown in black are trials which recovered the BE Zn isotope composition of $\varepsilon^{64}Zn_{BE} = 0.00 \pm 0.17$. The vertical line and grey shaded region represent the mean and 2sd of all successful trials ($x^{Zn}_{CC} = 0.48 \pm 0.15$).

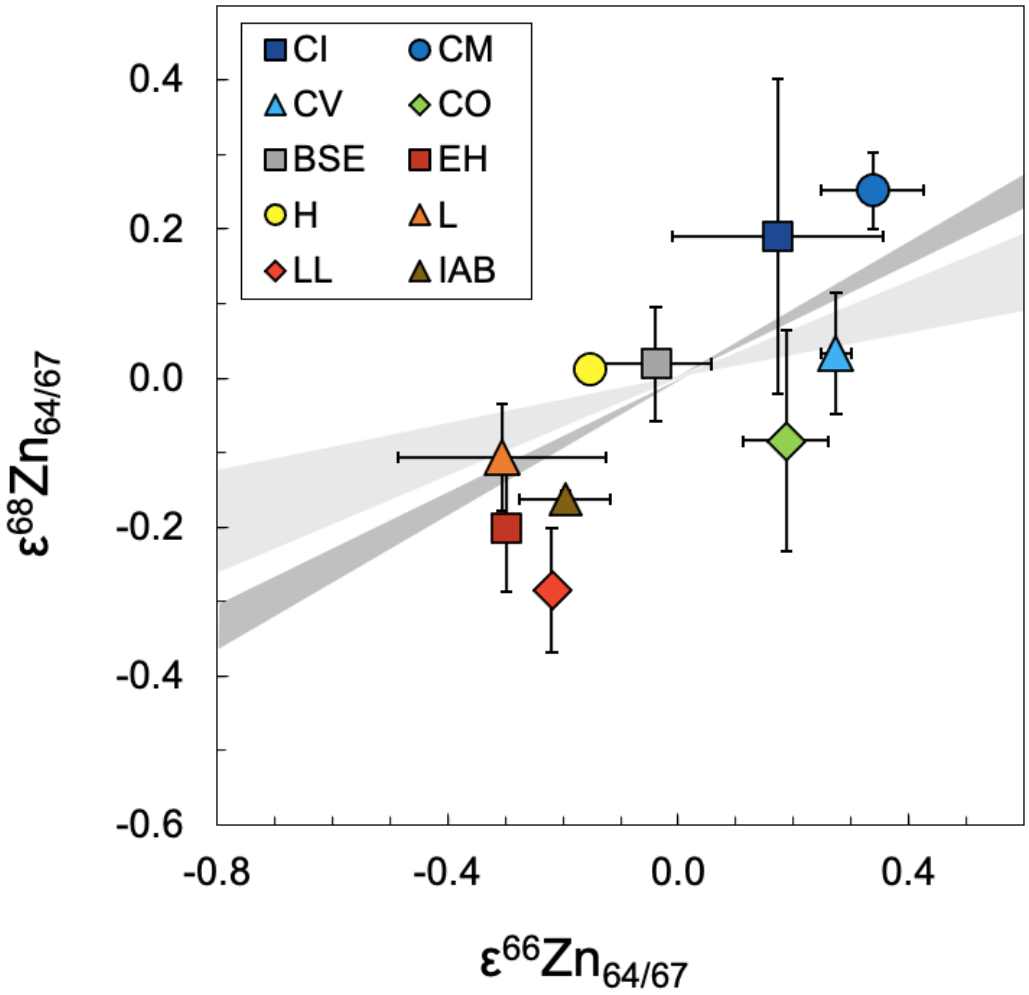


Figure S4. Plot of $\varepsilon^{66/67}Zn_{64/67}$ versus $\varepsilon^{68/67}Zn_{64/67}$ comparing our results with modeled anomalies. Same as Figure 2, but for data obtained using $^{64}Zn/^{67}Zn$ for mass bias normalization.

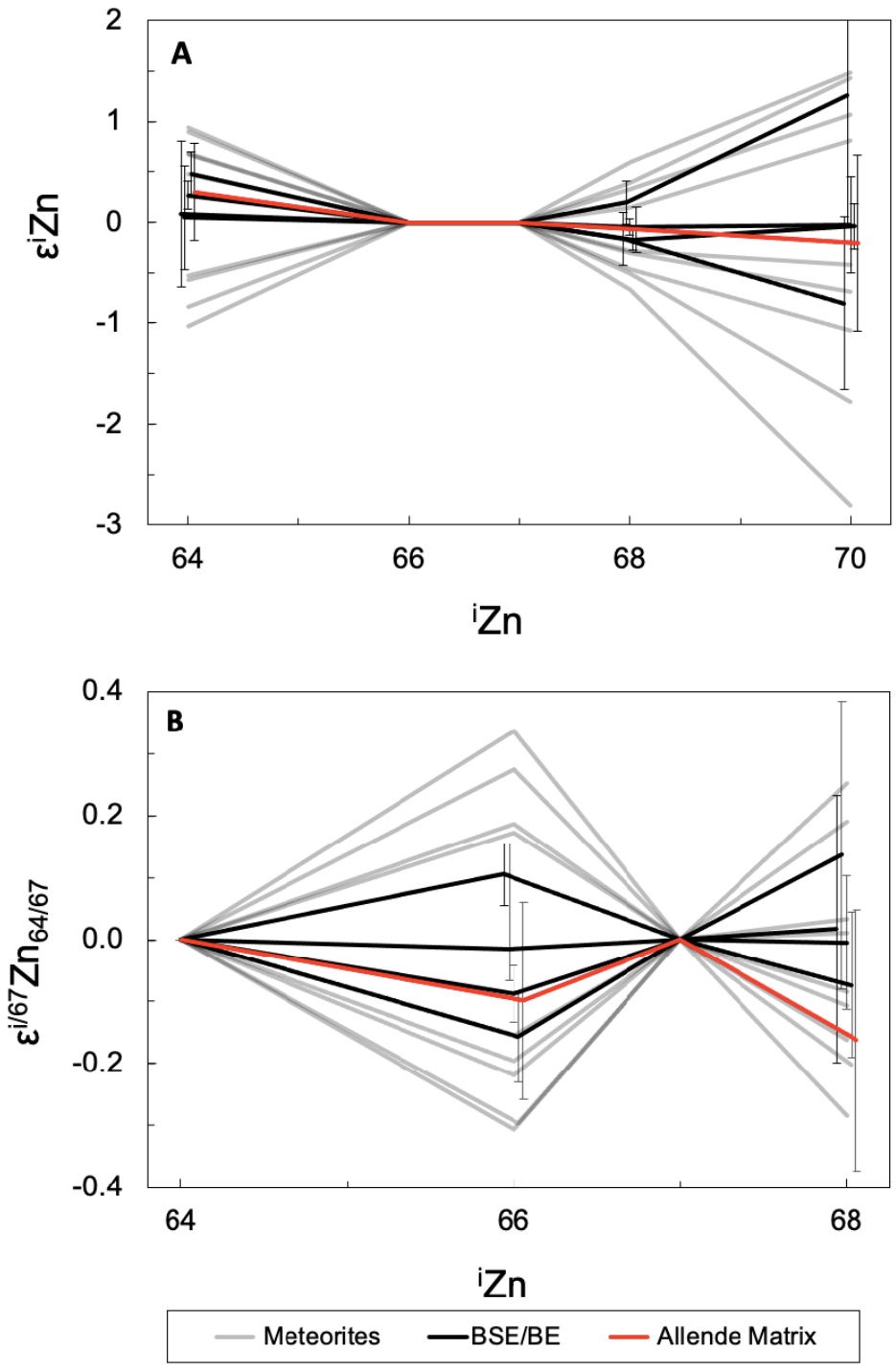


Figure S5. Mass independent Zn isotope compositions of BSE rocks. Shown are the mean (A) $\varepsilon^{i}Zn$ and (B) $\varepsilon^{i/67}Zn_{64/67}$ data for four BSE rocks (black) and Allende Matrix samples (red); error bars indicate ±2se. These five samples were repeatedly analyzed for quality control. Unlike the meteorites (plotted in light grey for comparison), the BSE rocks show either no or only barely resolvable deviations from εZn = 0, with an overall BSE mean that is identical to εZn = 0 within ±2se uncertainty (all data shown in Table S2).

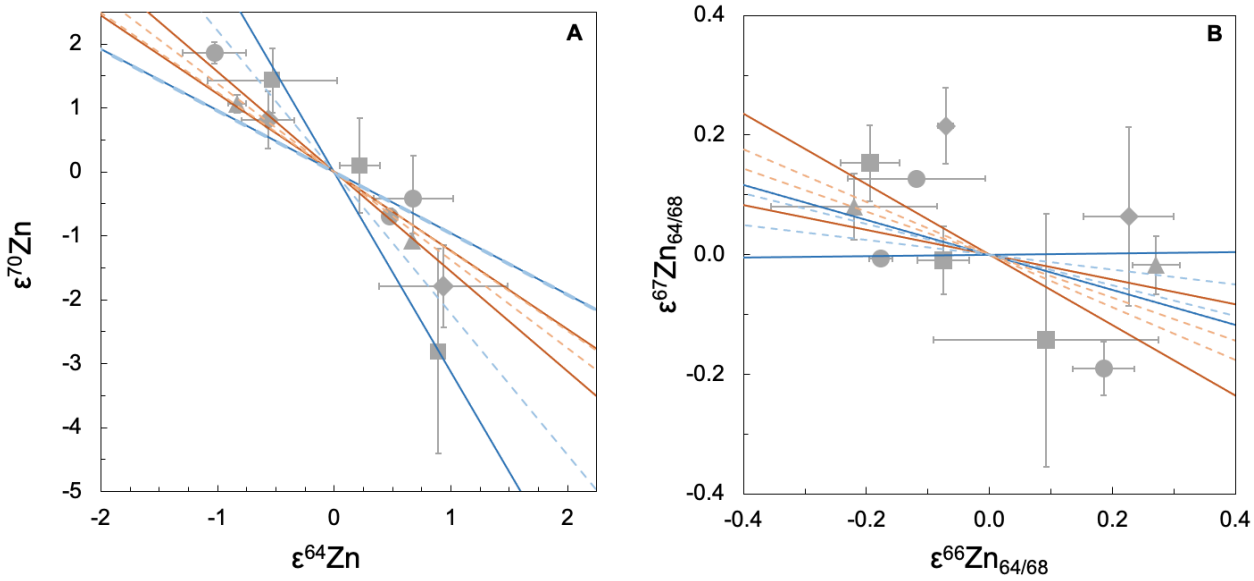


Figure S6. Modeled trendlines for predicted nucleosynthetic Zn isotope anomalies. (A) Correlation between $\varepsilon^{70}Zn$ and $\varepsilon^{64}Zn$ predicted by the addition of material from ECSNe [orange lines, (*30*)] and SNIa [blue lines, (*28*)]. The full lines were used to outline the grey fields in Figures 2, S4, and S9, as they encompass the results obtained for the other two variations of the respective models, shown by the dashed orange and blue lines. The meteorite data are shown in light grey for comparison. (B) same as (A), but for $\varepsilon^{67}Zn_{64/68}$ versus $\varepsilon^{66}Zn_{64/68}$.

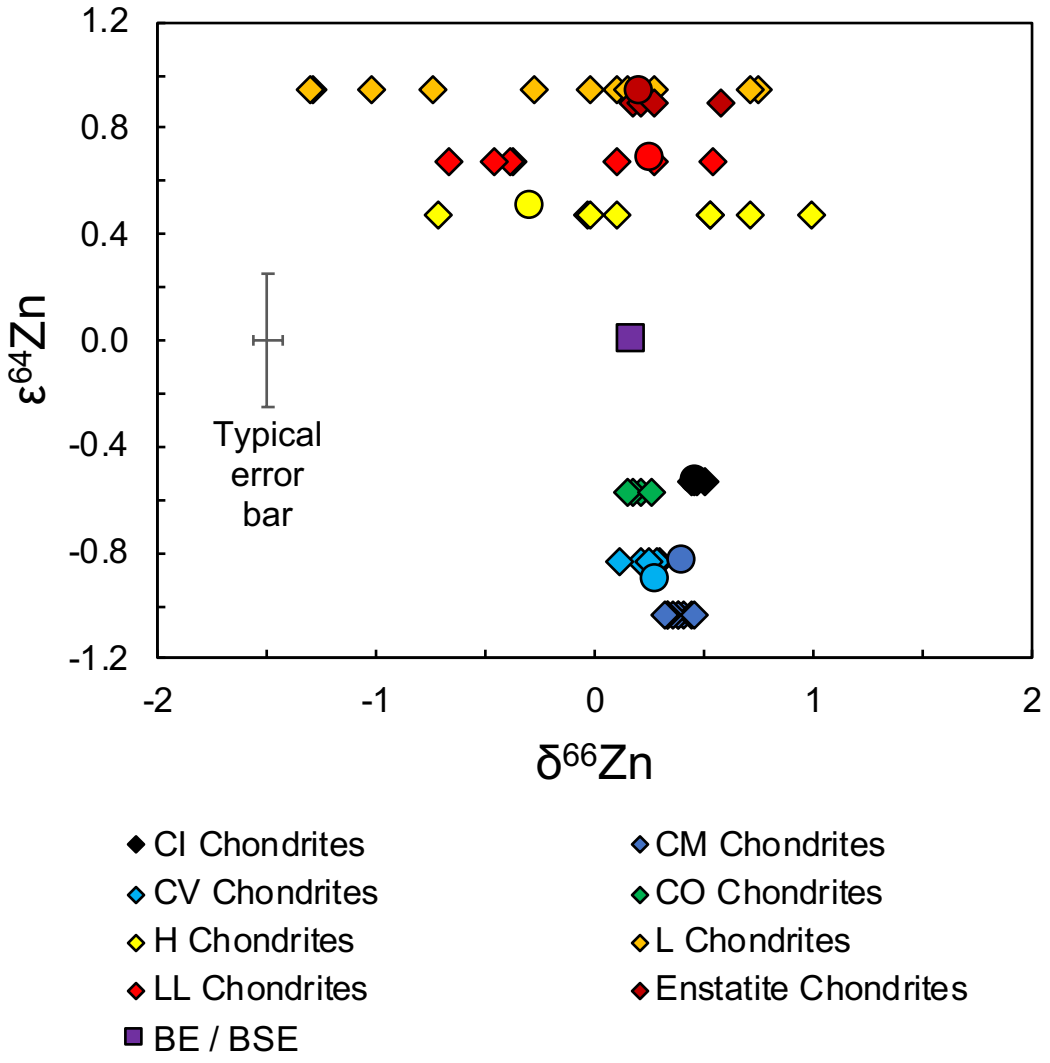


Figure S7. Mass dependent Zn isotope data ($\delta^{66}Zn$) and mass independent Zn isotope compositions ($\varepsilon^{64}Zn$) for chondrites. Circles are data for 7 meteorites that were analyzed both in this study and previously for $\delta^{66}Zn$ (Orgueil CI1; Murchison, Jbilet Winselwan, CM2; Allende CV3; Brownfield (1937) H3.7; Bishunpur LL3.1; Indarch EH4). For the meteorites shown as diamonds, the published $\delta^{66}Zn$ results were combined with the mean $\varepsilon^{64}Zn$ value of the respective meteorite group. The composition of the BE and BSE is $\delta^{66}Zn = 0.20‰$ (*74*) and $\varepsilon^{64}Zn = 0$ (this study). The 'typical error bar' denotes uncertainties of $\delta^{66}Zn = \pm 0.08‰$ (2sd) and $\varepsilon^{64}Zn = \pm 0.25$ (2se). The $\delta^{66}Zn$ data for meteorites are from (*36, 38, 43, 61, 62, 64-66*).

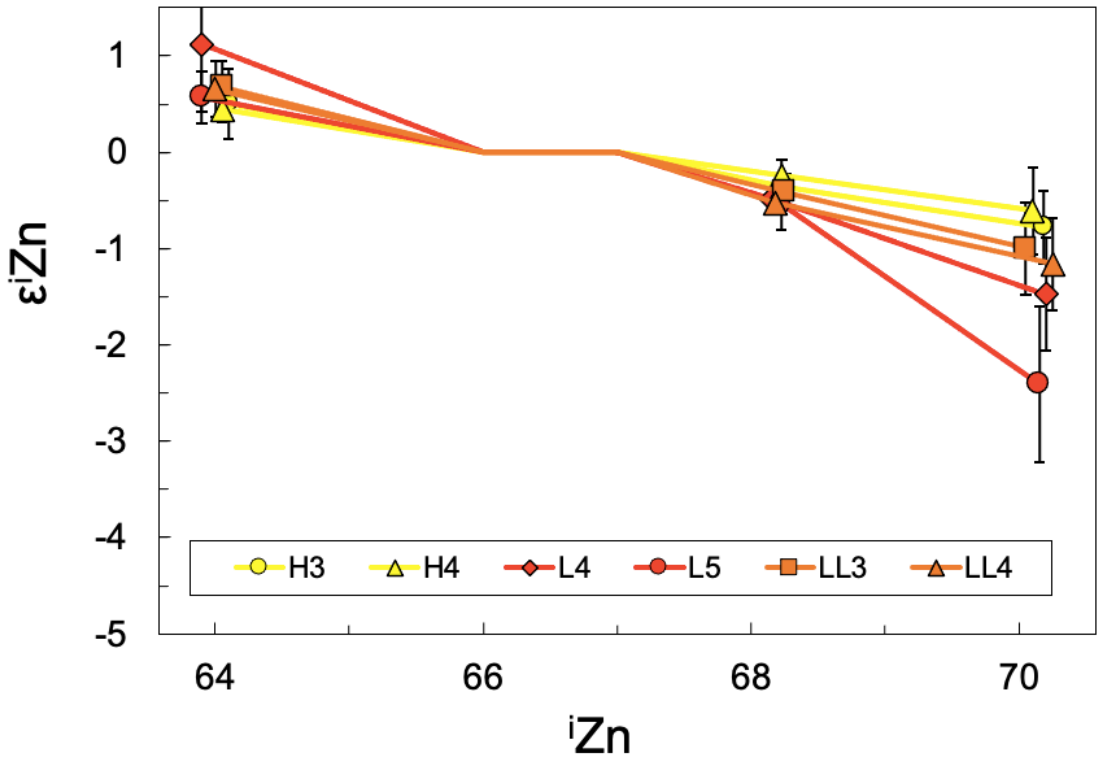


Figure S8. Mass independent Zn isotope data in ε^{i}Zn notation for the OCs. Shown are ε^{i}Zn data for H, L, and LL ordinary chondrites, which are further subdivided according to their petrographic grades. No analytically resolvable differences are observed for the meteorites of each group, regardless of their petrographic grade. Mass dependent Zn isotope data are available for two of the meteorites shown here and these have δ^{66}Zn values of –0.30 ± 0.05‰ (Brownfield (1937) H3.7) and 0.25 ± 0.05‰ (Bishunpur LL3.1) (*38*). The ε^{i}Zn data are listed in Table S2; error bars indicate ±2se.

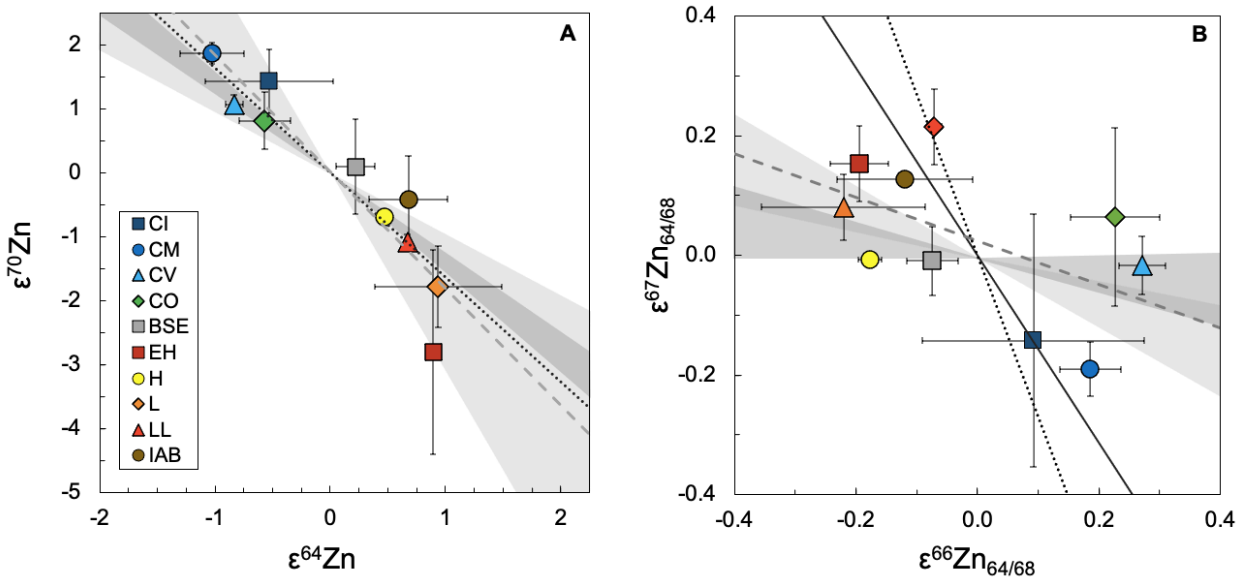


Figure S9. Mass independent Zn isotope data for the meteorite groups and BSE rocks. (A) Same as Figure 2, but now also showing the trend predicted by a NFSE model (black dotted line) using nuclear charge radii data from (*72*) and a best-fit trendline for the samples (dashed grey line). (B) Same as (A) but for εZn data obtained using $^{64}Zn/^{68}Zn$ for mass bias normalization and showing the trends for two NFSE models, which used the nuclear charge radii data of (*72*) and (*73*), as dotted and solid black lines, respectively. All modeled trends are compatible with the Zn isotope data determined using the $^{66}Zn/^{67}Zn$ normalization scheme (panel A). However, the majority of the measured meteorite data obtained using $^{64}Zn/^{68}Zn$ for internal normalization are not in accord with the steep trends predicted by the NFSE models, as the meteorites define a best-fit correlation (dashed line) with a more moderate slope (panel B). The data are from Table S2; error bars indicate ±2se.

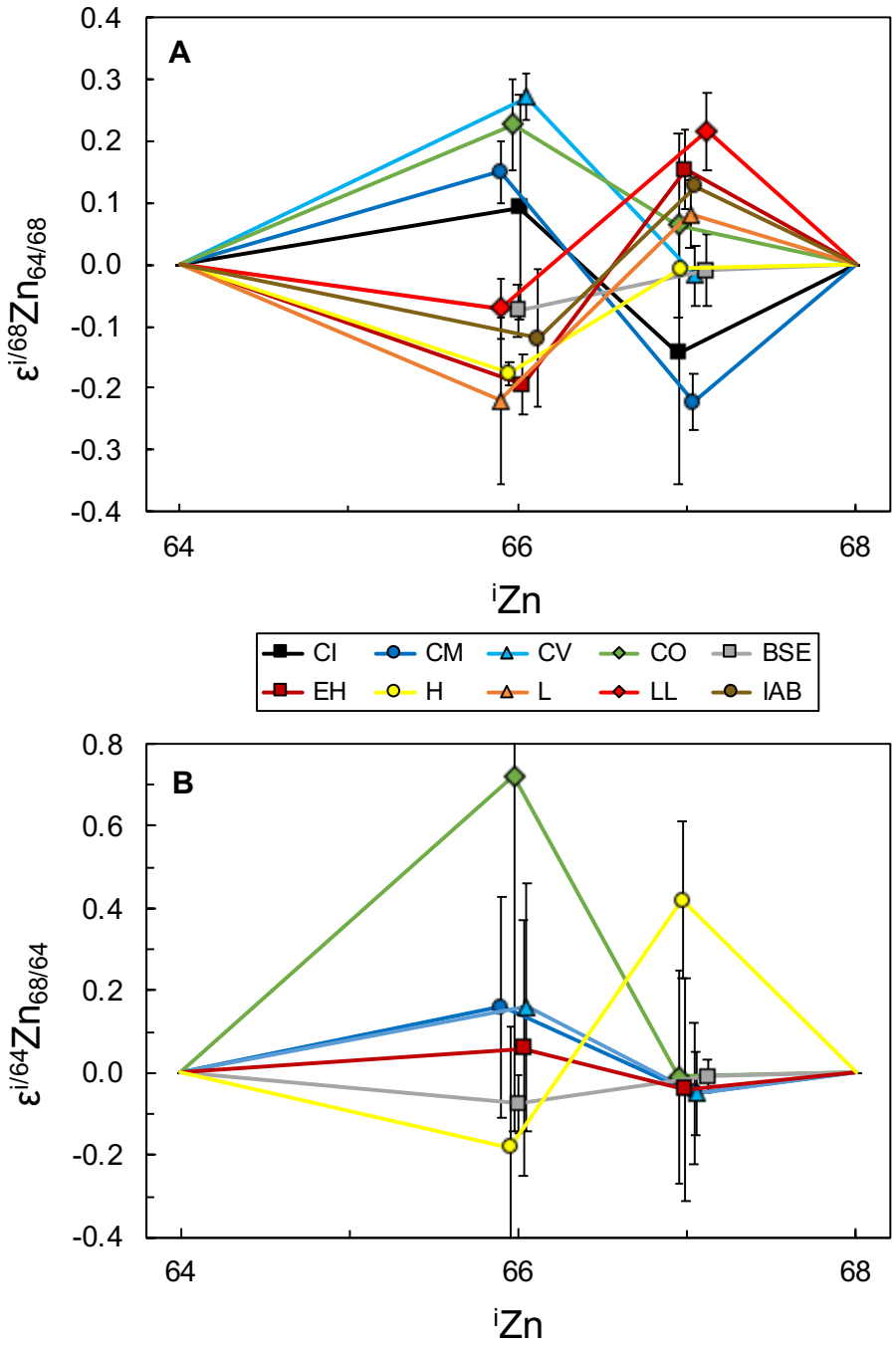


Figure S10. Mass independent Zn isotope data for meteorites and BSE rocks. Shown are (A) $\varepsilon^{i}Zn_{64/68}$ values from this study (Table S2) and (B) $\varepsilon^{i}Zn_{68/64}$ data from a previous investigation (*24*). As for the Zn isotope data normalized to $^{66}Zn/^{67}Zn$ and $^{66}Zn/^{68}Zn$, the results in panel (A) show that CCs and non-carbonaceous meteorites have complimentary Zn isotope patterns, albeit with more scatter due to larger uncertainties.

Table S1. Names, digested masses, identifiers and sources of the meteorites and BSE rocks analyzed in this study.

Samples	Type	Mass (g)	Identifier	Source
Meteorites				
Orgueil	CI1	0.158	BM.36104	Natural History Museum London
Jbilet Winselwan	CM2	1.82		Private collector [§]
Murchison	CM2	0.612	ME 2644, #26.55	Field Museum Chicago
Allende	CV3	2.255 to 2.480		Natural History Museum London
LAR 12002	CV3	0.253 *	LAR 12002.43	US Antarctic Meteorite Program [$]
NWA 4502	CV3	2.01		Private collector [§]
MIL 090025	CO3	0.251 *	MIL 090025.12	US Antarctic Meteorite Program [$]
NWA 13299	EH3	0.456		Private collector [§]
Indarch	EH4	1.302	M4 1403, #22	Field Museum Chicago
Brownfield	H3.7	2.03	MPI 113/1b	Senckenberg Museum für Naturkunde
Forest Vale	H4	0.62	USNM 4852	Smithsonian National Museum of Natural History
Saratov	L4	0.83	BM.1997	Natural History Museum London
Tennasilm	L4	2.00	USNM 483 2	Smithsonian National Museum of Natural History
Homestead	L5	1.03	BM.1962,157	Natural History Museum London
Bishunpur	LL3.1	0.213 *	BM.80339	Natural History Museum London
Soko Banja	LL4	1.47	BM.51857	Natural History Museum London
Canyon Diablo	IAB complex	8.46		Private collector [§]
Toluca [#]	IAB complex	10.8		Private collector [§]
BSE rocks				
BHVO-2	Hawaiian basalt			US Geological Survey
BTHO	Icelandic basalt			*(45)*
D-174	Gabbro (Dufek Intrusion)			*(46)*
P6Bt	Glacial till (W Greenland)			*(47)*

* The digested powder aliquots are from much larger (>2 g) homogenized powder samples. [#] Sample Toluca 2 is from (*48*). [$] US Antarctic meteorite samples are from the Antarctic Search for Meteorites (ANSMET) program funded by NSF and NASA; they are characterized and curated by the Dept. of Mineral Sciences of the Smithsonian Institution and the Astromaterials Curation Office at NASA Johnson Space Center. [§] Meteorite sources; Jbilet Winselwan: Gary Fujihara, Big Kahuna Meteorites; available at Center for Meteorite Studies, Arizona State University (ASU), Muséum National d'Histoire Naturelle Paris (MNHN), Institute of Meteoritics, University of New Mexico. NWA 4502: Mike Miller, Meteoritefinder.com; available at ASU, Research School of Earth Sciences, Australian National University. NWA 13299: Fabien Kuntz, WWMeteorites; available at Dept. of Geology, Appalachian State University. Canyon Diablo & Toluca: Mike Miller, Meteoritefinder.com; available at American Museum of Natural History, ASU, Field Museum Chicago, MNHN, Smithsonian National Museum of Natural History and numerous other collections.

Table S2. Mass independent Zn isotope data (in εZn notation) for the meteorites and BSE samples. m: number of sample digest aliquots processed separately through column chemistry. n is the total number of individual analytical runs for a given meteorite, for one or several powder/digest solution aliquots. x is the number of distinct meteorite/BSE samples in a group.

		Data normalised to $^{66}Zn/^{67}Zn$											
Sample		**$\varepsilon^{64/67}Zn$**	**2se**	**2sd**	**m/n**	**$\varepsilon^{68/67}Zn$**	**2se**	**2sd**	**m/n**	**$\varepsilon^{70/67}Zn$**	**2se**	**2sd**	**m/n**
Orgueil	CI1	-0.53	0.56	1.11	1/4	0.39	0.15	0.38	1/6	1.43	0.50	0.87	1/3
Jbilet Winselwan	CM2	-1.22	0.15	0.41	1/7	0.65	0.06	0.24	1/16	2.12	0.25	0.74	1/9
Murchison	CM2	-0.83	0.99	1.98	1/4	0.55	0.26	0.47	1/7	1.61	0.83	1.43	1/3
Allende	CV3	-0.91	0.21	1.52	8/51	0.36	0.15	1.33	8/82	0.91	0.60	3.33	8/31
LAR 12002	CV3	-0.85	0.28	0.83	1/9	0.33	0.19	0.71	1/14	1.19	0.21	0.46	1/5
NWA 4502	CV3	-0.74	0.23	0.90	2/16	0.28	0.08	0.43	2/28	1.12	0.25	0.85	2/12
MIL 090025	CO3	-0.57	0.22	0.67	1/9	0.15	0.16	0.61	1/15	0.81	0.45	1.10	1/6
CC mean (x=7)		-0.81	0.16	0.43	15/100	0.39	0.12	0.31	15/168	1.20	0.20	0.53	15/68
NWA 13299	EH3	0.85	0.34	1.06	1/10	-0.64	0.36	1.75	1/23	-3.93	1.68	6.07	1/13
Indarch	EH4	0.93	0.29	0.88	1/9	-0.70	0.16	0.61	1/15	-1.67	0.67	1.63	1/6
EC mean (x=2)		0.89	0.06	0.08	2/19	-0.67	0.05	0.07	2/38	-2.80	1.60	2.26	2/19
Brownfield (1937)	H3.7	0.50	0.37	0.90	1/6	-0.36	0.13	0.46	1/12	-0.78	0.38	0.92	1/6
Forest Vale	H4	0.44	0.13	0.49	1/14	-0.24	0.16	0.80	1/24	-0.61	0.45	1.43	1/10
Saratov	L4	0.63	0.11	0.39	1/14	-0.41	0.21	0.96	1/21	-1.89	0.72	1.91	1/7
Tennasilm	L4	1.61	0.61	1.05	1/3	-0.57	0.17	0.42	1/6	-1.06	0.77	1.33	1/3
Homestead	L5	0.57	0.27	0.72	1/7	-0.54	0.26	0.98	1/14	-2.41	0.81	2.14	1/7
Bishunpur	LL3	0.68	0.26	0.79	1/9	-0.41	0.13	0.50	1/15	-1.00	0.48	1.17	1/6
Soko Banja	LL4	0.66	0.30	1.02	2/12	-0.53	0.12	0.61	2/27	-1.16	0.48	1.84	2/15
OC mean (x=7)		0.73	0.28	0.74	8/77	-0.44	0.08	0.21	8/119	-1.27	0.45	1.19	8/54
NCC mean (x=9)		0.76	0.22	0.67	10/96	-0.49	0.09	0.27	10/157	-1.61	0.66	1.97	10/73
Canyon Diablo	IAB complex	0.92	0.36	1.13	1/10	-0.36	0.15	0.63	1/18	-0.89	0.27	0.77	1/8
Toluca	IAB complex	0.44	0.007	0.01	1/2	-0.21	0.13	0.25	1/4	0.06	0.06	0.08	1/2
NC meteorite mean (x=11)		0.75	0.19	0.64	12/96	-0.45	0.09	0.30	12/179	-1.39	0.62	2.04	12/83
BHVO-2	basalt	0.48	0.22	1.17	4/28	-0.18	0.10	0.65	4/39	-0.04	0.22	0.92	4/17
BTHO	basalt	0.08	0.72	1.62	6/35	-0.16	0.26	0.59	6/62	-0.80	0.86	2.10	6/27
D-174	gabbro	0.05	0.52	1.27	6/10	0.20	0.22	0.53	6/27	1.26	1.30	3.17	6/17
P6Bt	glacial till	0.27	0.14	0.69	3/16	-0.05	0.08	0.47	3/24	-0.02	0.47	1.64	3/8
Terrestrial mean (x=4)		0.22	0.17	0.34	19/89	-0.05	0.15	0.30	19/152	0.10	0.74	1.48	19/63
Allende Matrix		0.30	0.48	1.53	4/10	-0.07	0.22	0.99	4/20	-0.20	0.87	2.76	4/10

Continued on next page

Table S2 continued.

		Data normalised to $^{64}Zn/^{67}Zn$							
Sample		**$\varepsilon^{66/67}Zn$**	**2se**	**2sd**	**m/n**	**$\varepsilon^{68/67}Zn$**	**2se**	**2sd**	**m/n**
Orgueil	CI1	0.17	0.18	0.37	1/4	0.19	0.21	0.42	1/4
Jbilet Winselwan	CM2	0.40	0.05	0.14	1/7	0.22	0.13	0.33	1/7
Murchison	CM2	0.28	0.33	0.65	1/4	0.29	0.07	0.13	1/4
Allende	CV3	0.30	0.07	0.50	8/51	0.13	0.11	0.82	8/51
LAR 12002	CV3	0.28	0.09	0.28	1/9	-0.04	0.23	0.68	1/9
NWA 4502	CV3	0.24	0.07	0.30	2/16	0.01	0.09	0.37	2/16
MIL 090025	CO3	0.19	0.07	0.22	1/9	-0.08	0.15	0.45	1/9
CC mean (x=7)		0.27	0.05	0.14	15/100	0.10	0.10	0.26	15/100
NWA 13299	EH3	-0.29	0.10	0.32	1/10	-0.14	0.23	0.71	1/10
Indarch	EH4	-0.31	0.10	0.29	1/9	-0.26	0.14	0.41	1/9
EC mean (x=2)		-0.30	0.01	0.02	2/19	-0.20	0.08	0.12	2/19
Brownfield (1937)	H3.7	-0.16	0.12	0.30	1/6	0.01	0.15	0.37	1/6
Forest Vale	H4	-0.14	0.04	0.16	1/14	0.01	0.17	0.64	1/14
Saratov	L4	-0.21	0.03	0.13	1/14	-0.02	0.23	0.87	1/14
Tennasilm	L4	-0.53	0.20	0.34	1/3	-0.14	0.12	0.21	1/3
Homestead	L5	-0.19	0.09	0.24	1/7	-0.16	0.22	0.57	1/7
Bishunpur	LL3	-0.22	0.09	0.26	1/9	-0.23	0.16	0.47	1/9
Soko Banja	LL4	-0.22	0.10	0.34	2/12	-0.34	0.23	0.79	2/12
OC mean (x=7)		-0.24	0.09	0.24	8/65	-0.12	0.09	0.25	8/65
NCC mean (x=9)		-0.25	0.07	0.22	10/84	-0.14	0.08	0.23	10/84
Canyon Diablo	IAB complex	-0.29	0.10	0.50	1/10	-0.14	0.23	0.34	1/10
Toluca	IAB complex	-0.10	0.16	0.00	1/2	-0.16	0.21	0.04	1/2
NC meteorite mean (x=11)		-0.24	0.06	0.21	12/96	-0.15	0.06	0.21	12/96
BHVO-2	basalt	-0.16	0.07	0.39	4/28	-0.07	0.12	0.62	4/28
BTHO	basalt	0.11	0.05	0.10	6/35	0.02	0.22	0.43	6/35
D-174	gabbro	-0.02	0.17	0.42	6/10	0.14	0.25	0.61	6/10
P6Bt	glacial till	-0.09	0.05	0.23	3/16	-0.01	0.11	0.53	3/16
Terrestrial mean (x=4)		-0.04	0.10	0.19	19/89	0.02	0.08	0.15	19/89
Allende Matrix		-0.10	0.16	0.50	4/10	-0.16	0.21	0.67	4/10

Continued on next page.

Table S2 continued.

		Data normalised to $^{64}Zn/^{68}Zn$							
Sample		**$\varepsilon^{66/68}Zn$**	**2se**	**2sd**	**m/n**	**$\varepsilon^{67/68}Zn$**	**2se**	**2sd**	**m/n**
Orgueil	CI1	0.09	0.28	0.56	1/4	-0.14	0.16	0.31	1/4
Jbilet Winselwan	CM2	0.22	0.10	0.25	1/7	-0.16	0.10	0.27	1/7
Murchison	CM2	0.15	0.40	0.79	1/4	-0.22	0.05	0.10	1/4
Allende	CV3	0.23	0.05	0.36	8/51	-0.07	0.09	0.62	8/51
LAR 12002	CV3	0.31	0.15	0.46	1/9	0.03	0.17	0.51	1/9
NWA 4502	CV3	0.26	0.09	0.38	2/16	0.00	0.07	0.28	2/16
MIL 090025	CO3	0.23	0.09	0.26	1/9	0.06	0.11	0.34	1/9
CC mean (x=7)		0.21	0.05	0.14	15/100	-0.07	0.07	0.20	15/100
NWA 13299	EH3	-0.23	0.10	0.31	1/10	0.11	0.17	0.54	1/10
Indarch	EH4	-0.16	0.11	0.33	1/9	0.20	0.10	0.31	1/9
EC mean (x=2)		-0.19	0.05	0.07	2/19	0.15	0.06	0.09	2/19
Brownfield (1937)	H3.7	-0.19	0.15	0.37	1/6	-0.01	0.11	0.28	1/6
Forest Vale	H4	-0.16	0.07	0.27	1/14	-0.01	0.13	0.49	1/14
Saratov	L4	-0.21	0.13	0.49	1/14	0.01	0.18	0.66	1/14
Tennasilm	L4	-0.37	0.23	0.40	1/3	0.11	0.09	0.16	1/3
Homestead	L5	-0.08	0.13	0.35	1/7	0.12	0.16	0.43	1/7
Bishunpur	LL3	-0.08	0.11	0.32	1/9	0.17	0.12	0.36	1/9
Soko Banja	LL4	-0.06	0.16	0.55	2/12	0.26	0.17	0.60	2/12
OC mean (x=7)		-0.17	0.07	0.20	8/65	0.09	0.07	0.19	8/65
NCC mean (x=9)		-0.17	0.06	0.18	10/84	0.11	0.06	0.18	10/84
Canyon Diablo	IAB complex	-0.20	0.08	0.24	1/10	0.13	0.07	0.23	1/10
Toluca	IAB complex	-0.04	0.00	0.00	1/2	0.13	0.02	0.03	1/2
NC meteorite mean (x=11)		-0.16	0.05	0.18	12/96	0.11	0.05	0.16	12/96
BHVO-2	basalt	-0.12	0.11	0.56	4/28	0.06	0.09	0.47	4/28
BTHO	basalt	-0.01	0.15	0.36	6/35	0.01	0.15	0.30	6/35
D-174	gabbro	-0.08	0.08	0.18	6/10	-0.10	0.19	0.46	6/10
P6Bt	glacial till	-0.08	0.09	0.02	3/16	0.00	0.08	0.08	3/16
Terrestrial mean (x=4)		-0.07	0.04	0.08	19/89	-0.01	0.06	0.11	19/89
Allende Matrix		-0.04	0.10	0.30	4/10	0.12	0.16	0.50	4/10

Table S3. Zn concentration data (in µg g^{-1}) for CCs, ECs, OCs and Earth reservoirs compiled from the literature and adopted in this study.

CC	CI	CM	CV	CO
(*68*)	312			
(*2*)	312	185	116	100
(*69*)	310			
(*1*)	315	180	110	110
(*70*)	323			
(*71*)	321-391	197	123	110
This study (adopted)	**320**	**185**	**115**	

Earth	BSE	Core	BE	Core/BSE
(*69*)	55			
(*72*)	55	(10)	40	0.17
(*70*)	54			
(*71*)	55	50	52	0.91
(*73*)	54	29	46	0.54
(*64*)	55	101	70	1.84
This study (adopted)	**54**	**12-103**	**40-70**	**0.2-1.9**

EC	EH3,4	EH5	EL3	EL5,6
(*2*)	250		17	
(1)	290		18	
(*74*)	90-519	44-501		7.5-86
(*75*)	62-342	21-290		10-23
(*76*)	112-379	372	209-218	117

OC	H	L	LL
(*2*)	47	50	46
(*1*)	47	57	56
(*74*)			44-81
(*37*)	40-48	40-79	40-52
(*77*)	17-158	14-109	

Table S4. Ion exchange column chemistry for Stage 1 of the Zn separation from meteorite and rock samples. The separation used either large quartz glass columns with 2 ml resin beds (of 6 mm diameter) and a reservoir volume (RV) of 50 ml or small Teflon columns with 250 µl resin beds, with a bed height and diameter of about 25 mm and 3.5 mm, respectively.

Reagent	Quartz Columns Volume (ml)	Teflon Columns Volume (µl)	Effect
AG 1X8 100-200 mesh resin	2	250	Add resin slurry in 0.1 M HCl
2 M HNO_3	15	2 x RV	Clean resin
H_2O	2	1000	Clean resin
6 M HCl	26	1 x RV	Convert resin to Cl^- form
0.5 M HCl	12		Resin conditioning
3 M HCl	6	600	Resin equilibration
Sample in 3 M HCl	10	1000-2000	Sample loading; elution of Mg, Al, S, Ti, V, Cr, Fe, Ge, Ba
3 M HCl	2	200	Elution incl. Mg, Al, S, Ti, V, Cr, Fe, Ge, Ba
0.5 M HCl	30	3000	Elution incl. Mg, Al, S, Ti, V, Cr, Fe, Ge, Ba
1 M HCl	10	1000	Matrix elution (e.g., Mo)
2 M HCl	12	1000	Matrix elution
6 M HCl	16	1500	Matrix elution (e.g., Ag)
0.1 M HBr + 0.5 M HNO_3	20	3000	Elution of Zn

Table S5. Ion exchange column chemistry for Stages 2 and 3 of the Zn separation from meteorite and rock samples. The separation was carried out in Teflon shrink-fit columns with a reservoir volume (RV) of 2 ml and a resin volume of about 250 µl, with a bed height and diameter of about 25 mm and 3.5 mm, respectively.

Reagent	Volume (µl)	Effect
AG MP1 100-200 mesh resin	250	Add resin slurry in 0.1 M HCl
0.1 M HNO_3	2 x RV	Clean resin
H_2O	1000	Clean resin
6 M HCl	3000	Convert resin to Cl^- form
1 M HCl	2000	Resin equilibration
Sample in 1 M HCl	1000	Sample loading; elution of Mg, Al, S, Ti, V, Cr, Fe, Ge, Ba
1 M HCl	8000	Elution of Mg, Al, S, Ti, V, Cr, Fe, Ge, Ba
0.01 M HCl	7000	Elution of Zn

Table S6. Operating conditions of the Nu Plasma MC-ICP-MS and the Nu Instruments DSN 100 desolvating sample introduction system.

Nu Plasma II MC-ICP-MS	
RF Power	1300 W
Acceleration potential	6000 V
Ar coolant gas flow	13 l min^{-1}
Ar auxiliary gas flow	1 l min^{-1}
Expansion chamber vacuum	~0.75 mbar
Analyser vacuum	~2 x 10^{-9} mbar
Faraday cup resistors	10^{11} Ω
Sensitivity for Zn	230 – 420 V (µg ml^{-1})$^{-1}$

Nu Instrument DSN-100 desolvating nebulizer system	
Spray chamber temperature	110°C
Desolvator temperature	160°C
Argon sweep gas	~3.4 to 5 l min^{-1}
Nebuliser pressure	~60 psi
Sample uptake rate	~120 µl min^{-1}

Table S7. Collector configurations that were used for the Zn isotope measurements, abundances of the isotopes of Zn as well as spectral interferences from isobars, Ba^{2+} and the most relevant molecular ions.

Faraday collector	**L4**	**L2**	**Ax**	**H1**	**H2**	**H4**	**H6**	**H7**	**H8**
Collector configuration M64	^{62}Ni	^{64}Zn			^{66}Zn	^{67}Zn	^{68}Zn	$^{137}Ba^{2+}$	
Isotope abundance Zn		49.2%			27.7%	4.0%	18.5%		
Isotope abundance Ni	3.6%	0.1%							
Isotope abundance Ba^{2+} ions					0.1%	2.4%	7.9%	11.2%	
Collector configuration M70	^{66}Zn	^{67}Zn	^{68}Zn	$^{137}Ba^{2+}$		^{70}Zn			^{72}Ge
Isotope abundance Zn	27.7%	4.0%	18.5%			0.6%			
Isotope abundance Ge						20.5%			27.5%
Isotope abundance Ba^{2+} ions	0.1%	2.4%	7.9%	11.2%					

Mass number	**62**	**64**	**66**	**67**	**68**	**68.5**	**70**	**72**
Collector configuration M64	L4	Ax	H2	H4	H6	H7		
Collector configuration M70			L4	L2	Ax	H1	H4	H8
Zn^{+} ions		49.2%	27.7%	4.0%	18.5%		0.6%	
Ni^{+} ions	3.6%	0.9%						
Ge^{+} ions							20.5%	27.5%
Ba^{2+} ions			0.1%	2.4%	7.9%	11.2%		
MgAr		80.0%	11.0%					
AlAr				100%				
SiAr					92.2%		3.1%	
SAr								95.0%
TiO	8.2%	73.7%	5.2%					
VO			0.2%	99.8%				
CrO			4.3%		83.8%		2.4%	
FeO							5.8%	91.8%

Table S8. Ti and Cr isotope data utilized in Figure S2. The ε^{50}Ti data are from (*34*) and (*60*). The ε^{54}Cr data are from (*29*).

Sample	$\varepsilon^{50/47}$Ti	2se	$\varepsilon^{54/52}$Cr	2se
Orgueil (CI)	1.85	0.03	1.65	0.07
CI mean	1.85	0.03	1.65	0.07
Murchison (CM2)	3.09	0.08	0.97	0.20
Murray (CM2)	2.84	0.05		
CM mean	3.09	0.08	0.97	0.20
Allende (CV3)	4.23	0.77	0.95	0.10
Leoville (CV3)			0.71	0.15
Vigarano (CV3)			0.87	0.09
CV mean	4.20	0.61	0.87	0.08
Kainsaz (CO3.2)			0.87	0.18
Lancé (CO3)	3.46	0.10		
Ornans (CO3)	3.37	0.09		
Isna (CO3)	3.50	0.06		
Félix (CO3)	4.69	0.12		
CO mean	3.76	0.54		
ALHA 77295 (EH3)			0.05	0.14
Indarch (EH4)	-0.13	0.05	0.05	0.14
QUE 94204 (EH7)			0.21	0.08
Qingzhen (EH3)	-0.12	0.20		
Sahara 97072 (EH3)	-0.15	0.06		
Adhi Kot (EH4)	-0.10	0.04		
Abee (EH4)	-0.06	0.04		
Saint-Sauveur (EH5)	-0.15	0.09		
EH mean	-0.12	0.03	0.03	0.14
LAP 03601 (H4)			-0.28	0.11
Kesen (H4)	-0.37	0.05		
Juancheng (H5)	-0.60	0.08		
St Severin (H6)	-0.74	0.20		
H mean	-0.58	0.14	-0.28	0.11
QUE 97008 (L3)			-0.42	0.14
Hedjaz (L3.7)	-0.65	0.13		
Ausson (L5)	-0.64	0.03		
Isoulane-n-Amahar (L6)	-0.59	0.05		
L mean	-0.63	0.03	-0.42	0.14
Dar al Gani (LL3)	-0.72	0.16		
Krymka (LL3.2)	-0.66	0.05		
GRO 95552 (LL4)			-0.33	0.10
Paragould (LL5)	-0.61	0.07		
LL mean	-0.66	0.05	-0.33	0.10

Table S9. Mean $\varepsilon^{64}Zn$, $\varepsilon^{70}Zn$, and $\varepsilon^{66/67}Zn_{64/67}$ values of endmembers used in the mass balance calculations and their respective p-values. n is the number of meteorite groups included in each endmember. The p-values are from ANOVA tests which compared the εZn values of all meteorites (from different groups) that contribute to a given endmember.

Endmembers	$\varepsilon^{64}Zn$	2se	2sd	p-value	$\varepsilon^{70}Zn$	2se	2sd	p-value	$\varepsilon^{66/67}Zn_{64/67}$	2se	2sd	p-value	n
CI-CM-CO-CV	-0.81	0.16	0.43	0.23	1.20	0.20	0.53	0.09	0.27	0.05	0.01	0.22	4
CI-CM	-0.86	0.33	0.56	0.38	1.47	0.12	0.20	0.51	0.28	0.11	0.19	0.37	2
CO-CV	-0.77	0.13	0.26	0.11	1.01	0.15	0.31	0.26	0.25	0.04	0.08	0.11	2
EC-OC-IAB	0.75	0.19	0.64	0.68	-1.39	0.62	2.04	0.12	-0.24	0.06	0.21	0.60	5
EC-OC	0.76	0.22	0.67	0.57	-1.61	0.66	1.97	0.18	-0.25	0.07	0.22	0.56	4
OC	0.73	0.28	0.74	0.52	-1.27	0.45	1.19	0.15	-0.24	0.09	0.24	0.52	3
EC	0.89	0.06	0.08	-	-2.80	1.60	2.26	-	-0.30	0.01	0.02	-	1

.

Table S10. Estimates for the fraction of Zn derived from CC material, x_{CC}^{Zn}, from mass balance models. Results are from Monte Carlo simulations that employ different combinations of CC and NC endmembers and one of three selected isotope ratios. All results are indistinguishable within uncertainties, suggesting that the selection of endmembers or isotope ratio does not substantially impact the outcome of the models.

	$\varepsilon^{64}Zn$		$\varepsilon^{70}Zn$		$\varepsilon^{66/67}Zn_{64/67}$	
Endmembers	x^{Zn}_{CC}	2sd	x^{Zn}_{CC}	2sd	x^{Zn}_{CC}	2sd
CI-CM-CO-CV + EC-OC-IAB	0.48	0.15	0.57	0.33	0.49	0.25
CI-CM-CO-CV + EC-OC	0.48	0.15	0.53	0.35	0.48	0.25
CI-CM + OC	0.46	0.18	0.45	0.33	0.45	0.28
CI-CM + EC	0.52	0.14	0.63	0.29	0.53	0.23
CO-CV + OC	0.53	0.12	0.55	0.40	0.48	0.28
CO-CV + EC	0.48	0.18	0.69	$^{+0.31}_{-0.33}$	0.56	0.22

Table S11. Estimates for the mass fraction of CC material accreted by the Earth, x_{CC}, from mass balance models. Same as Table S10, but for the total mass fraction of CC material accreted by Earth, rather than the Zn mass fraction.

	$\varepsilon^{64}Zn$		$\varepsilon^{70}Zn$		$\varepsilon^{66/67}Zn_{64/67}$	
Endmembers	x_{CC}	2sd	x_{CC}	2sd	x_{CC}	2sd
CI-CM-CO-CV + EC-OC-IAB	0.13	0.10	0.15	0.14	0.14	0.16
CI-CM-CO-CV + EC-OC	0.13	0.10	0.14	0.14	0.13	0.12
CI-CM + OC	0.13	0.10	0.13	0.13	0.13	0.12
CI-CM + EC	0.14	0.11	0.18	0.15	0.15	0.12
CO-CV + OC	0.15	0.11	0.15	0.16	0.16	0.19
CO-CV + EC	0.13	0.10	0.19	0.16	0.13	0.13